



HAL
open science

High power ultralow-intensity noise continuous wave laser tunable from orange to red

Dia Darwich, Roopa Prakash, Clément Dixneuf, Yves-Vincent Bardin,
Mathieu Goeppner, Germain Guiraud, Nicholas Traynor, Giorgio Santarelli,
Adèle Hilico

► **To cite this version:**

Dia Darwich, Roopa Prakash, Clément Dixneuf, Yves-Vincent Bardin, Mathieu Goeppner, et al.. High power ultralow-intensity noise continuous wave laser tunable from orange to red. *Optics Express*, 2022, 30 (8), pp.12867. 10.1364/OE.455218. hal-04690846

HAL Id: hal-04690846

<https://hal.science/hal-04690846v1>




Submitted on 6 Sep 2024

HAL is a multi-disciplinary open access archive for the deposit and dissemination of scientific research documents, whether they are published or not. The documents may come from teaching and research institutions in France or abroad, or from public or private research centers.

L'archive ouverte pluridisciplinaire **HAL**, est destinée au dépôt et à la diffusion de documents scientifiques de niveau recherche, publiés ou non, émanant des établissements d'enseignement et de recherche français ou étrangers, des laboratoires publics ou privés.



High power ultralow-intensity noise continuous wave laser tunable from orange to red

DIA DARWICH,^{1,*}  ROOPA PRAKASH,¹ CLÉMENT DIXNEUF,² 
YVES-VINCENT BARDIN,² MATHIEU GOEPNER,² GERMAIN
GUIRAUD,² NICHOLAS TRAYNOR,² GIORGIO SANTARELLI,¹  AND
ADÈLE HILICO¹

¹LP2N, IOGS, CNRS and Université de Bordeaux, rue François Mitterrand, 33400 Talence, France

²Azur Light Systems, 11 Avenue de Canteranne, 33600 Pessac, France

*dia.darwich@institutoptique.fr

Abstract: We report here on the development of a multi-Watt power tunable single frequency ultra-low noise laser system emitting around 620 nm. More than 5 W of output power is obtained between 616.5 nm and 630.8 nm using sum frequency generation of 1050 nm and 1550 nm tunable laser sources in a periodic poled lithium niobate crystal. The tunability is achieved through temperature and channel shift, and only limited by the crystal characteristics. An output power of 10.1 W and an optical-optical efficiency of 45% are reached at 624.5 nm. The relative intensity noise properties of the conversion process have been experimentally investigated in different configurations showing excellent agreement with the analytical prediction.

© 2022 Optica Publishing Group under the terms of the [Optica Open Access Publishing Agreement](#)

1. Introduction

The development of high-power single-frequency laser with a wavelength emission between 600 nm and 640 nm becomes essential for several applications such as single molecule spectroscopy [1] or for high power UV generation for quantum applications [2–7], especially, direct Rydberg excitation of arrays of atoms for quantum computing applications [8,9]. There are very few industrial solutions to produce such sources. Dye lasers [6,7] directly emit in this spectral range, however the output power of these systems is limited to few hundreds of mW and their maintenance is complex, especially for Continuous Wave (CW) operation. Another solution is to realize an optical parametric oscillator, but it requires a cavity that will affect the noise of the laser, and it must be pumped by a costly high power visible laser [10]. A relatively simple, easy to maintain and effective technique to produce high power red radiation is through Sum Frequency Generation (SFG). This technique is based on the mixing of two lasers at 1 μm and 1.5 μm wavelengths using a nonlinear crystal. The SFG power depends on the power at 1 μm and 1.5 μm and also on the conversion efficiency, which depends mainly on two properties: the nonlinear coefficient (d_{eff}) and the length of the chosen crystal. Due to their high d_{eff} (>15 pm/V), and their length which can go up to more than 40 mm, Periodic Poled Lithium Niobate (PPLN) crystals represent excellent frequency conversion media. The orientation of the lithium niobate crystal is periodically inverted to prevent the phase mismatch between the photons during propagation, yielding a high conversion efficiency. The poling period to reach the quasi-phase matching condition depends on the interacting wavelengths and the temperature of the crystal. Moreover, when 5% of MgO is added to PPLN (MgO PPLN), the operating temperature range is extended (from ambient temperature up to 200 °C) [11] by mitigating the photorefractive effects, which makes the MgO PPLN crystals excellent candidates for high power tunable lasers applications. In [12,13], more than 20 W at 780 nm with 45% efficiency have been generated via Second Harmonic Generation (SHG) using an MgO PPLN crystal. However, the maximum output power achieved within the entire red spectrum is still below 9 W [14] and this laser

operates at a fixed wavelength for a specific application (637 nm with 38% efficiency). To our knowledge, the only demonstration of a tunable single frequency system is from Bridge et al. [4] and has demonstrated a tunability of 6 nm at 635 nm with a maximum output power of 1.6 W using a PP SLT (Stoichiometric Lithium Tantalate) crystal.

In this work, we demonstrate a tunability from 616.5 nm to 630.8 nm (14.3 nm) with an output power exceeding 5 W over the entire tuning range using a 40 mm MgO PPLN crystal. To the best of our knowledge, this is the widest tunability that has been demonstrated in single frequency regime at high power. Moreover, we demonstrate more than 10 W output power at 624.5 nm with an optical-optical efficiency of 45%. Additionally, and for the first time in this spectral domain, the Relative Intensity Noise (RIN) of the SFG is investigated at different wavelengths and in different configurations showing a value as low as -157 dB/Hz at 5 MHz. The tunability and the ultra-low intensity noise properties are achieved thanks to the development of widely tunable fiber Master Oscillator Power Amplifier (MOPAs) at 1040 nm and 1550 nm with an excellent spectral and noise quality.

2. Experimental setup

A schematic representation of the experimental setup is shown in Fig. 1. The 1040 nm tunable laser architecture is seeded by a tunable single frequency laser source (TOPTICA DL pro) emitting 30 mW between 1010 nm and 1083 nm with a 30 kHz linewidth. The homemade two-stage amplifier, which is based on commercially available double cladding Ytterbium-doped fibers pumped at 976 nm, delivers more than 10 W after isolator. Concerning the 1550 nm laser architecture, a 47 mW single frequency laser source (Pure Photonics PPCL300) emitting between 1525 nm and 1580 nm with a linewidth of 18 kHz is used to seed our homemade two-stage Erbium/Ytterbium-based MOPA. It can amplify the input signal to up to 10 W after isolator. In this MOPA, described in detail in [15], an Amplified Spontaneous Emission (ASE) filter is added between the two-amplification stages to achieve high Optical Signal to Noise Ratio (OSNR) after the second amplification stage. All fibers used in this work are polarization-maintaining fibers which ensure the emission of a linearly polarized beam with a Polarization Extinction Ratio (PER) exceeding 20 dB.

The optical spectra emitted by the 1050 nm MOPA (pump 1) and the 1550 nm MOPA (pump 2) at 10 W output power are represented in Fig. 2(a) and Fig. 2(b) respectively. These spectra are measured using an Optical Spectrum Analyzer (OSA, 600 nm – 1700 nm) with a resolution bandwidth of 0.1 nm and a span over 100 nm. At 1 μm , 10 W of output power is obtained between 1030 nm and 1070 nm (40 nm) with an OSNR higher than 40 dB over the entire emission band. The power at 1030 nm was limited to 10 W because of the ASE level which increases for a higher pump power and degrades the RIN quality [16,17], while we can achieve 12 W of output power at central wavelengths (\sim 1042 nm) and preserve an excellent RIN quality. The 1.5 μm MOPA ensures 10 W emission from 1533 nm to 1571 nm (38 nm) with a minimum OSNR of 38 dB at 1533 nm. Between 1545 nm and 1565 nm, the output power can be boosted up to 11 W.

It is worth noting that the output isolator of each MOPA is cleaved with an angle of 8° to avoid any parasitic reflection which can damage or degrade the amplifier. After isolator, the 1040 nm beam is collimated with a waist diameter of 1.04 mm using an 8 mm focal length lens (L1), while the 1550 nm is collimated with a waist diameter of 1.25 mm using a 6.2 mm focal length (L2). For a better alignment precision, the fibers and lenses are mounted on 3-dimensional (3D) translation stages.

The 1 μm (blue arrow in Fig. 1) and the 1.5 μm (black arrow in Fig. 1) are superimposed using the dichroic mirror DM1 (HR at 1.5 μm and HT at 1 μm). Thereafter, the collimated beams are focused, using a 60 mm focusing lens, into commercially available MgO doped Lithium Niobate with three periodically poled gratings (MgO PPLN, MSFG626 Covesion). The nonlinear crystal is 40 mm long, 0.5 mm thick and 10 mm wide. The three channels have a poling pitch (Λ) of 11.22

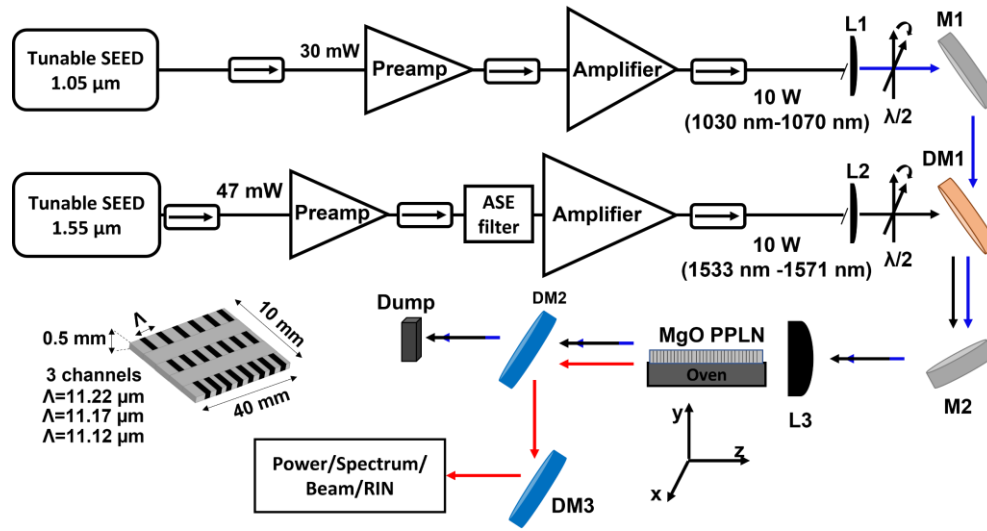


Fig. 1. Schematic representation of the experimental setup. L1, L2, and L3 are plano-convex lenses with focal lengths of 8 mm, 6.2 mm, and 60 mm respectively. M1 and M2 are silver mirrors. DM1 is a dichroic mirror with high transmission at 1 μm and high reflectivity at 1.5 μm . $\lambda/2$ are half-wave plates. DM2 and DM3 are dichroic mirrors with high reflectivity/transmission below/beyond 900 nm. In inset: Schematic representation for the used MgO PPLN crystal (not to scale).

μm , 11.17 μm and 11.12 μm and they are separated by 0.2 mm of unpoled region. A schematic representation of the used crystal is represented in the inset of Fig. 1 (the scales are adjusted to ensure clear representation). The periodically poled crystal is of type 0, thus both pump beams should be vertically polarized to obtain the best conversion efficiency and the generated red light will preserve the same polarization state. Each pump polarization is controlled by rotating a half-wave plate. Besides the polarization state and the beam overlap, the conversion efficiency depends on the waist size at the center of the crystal. Boyd and Kleinman have demonstrated that an optimum conversion efficiency is obtained when the focusing parameter $\xi=L/b$ is 2.84 [18] where 'L' is the crystal length and $b=2\times Z_R$ with ' Z_R ' the Rayleigh length, related the waist radius ' w_0 ' following the equation $Z_R=(n\times\pi\times w_0^2)/\lambda$ where 'n' is the refractive index of the crystal at the wavelength ' λ '. In our work, L is 40 mm, n is 2.2 at 1030 nm and reduces to 2 at 1550 nm (these values are obtained using the Sellmeier equation [19]) which gives us an optimal waist radius of 34 μm at 1040 nm and 42 μm at 1550 nm. In our setup, the focal lengths of L1 (8 mm), L2 (6.2 mm), and L3 (60 mm) were purposely chosen to obtain a waist radius of 37 μm and 47 μm at 1040 nm and 1550 nm respectively, corresponding to ξ of 2.2, without requiring any additional telescope. The careful alignment is realized by moving both the beams and the crystal which is mounted on a 3D translation stage.

To separate the generated red emission from the remaining pumps, two dichroic mirrors DM2 and DM3 with cut-on wavelengths of 900 nm were used. In the following, the red emission is investigated in terms of output power, beam quality, optical spectrum and RIN.

In order to reach the Quasi-Phase Matching (QPM) condition for the different wavelengths, the temperature of the MgO PPLN crystal was adjusted using a commercially available oven and temperature controller (Covesion). The oven temperature can be varied from 30 $^{\circ}\text{C}$ up to 250 $^{\circ}\text{C}$ with a resolution of 0.1 $^{\circ}\text{C}$. This temperature resolution is sufficient to reach and maintain the QPM of the crystal which has a Full-Width Half-Maximum (FWHM) of 1.1 $^{\circ}\text{C}$. This FWHM has

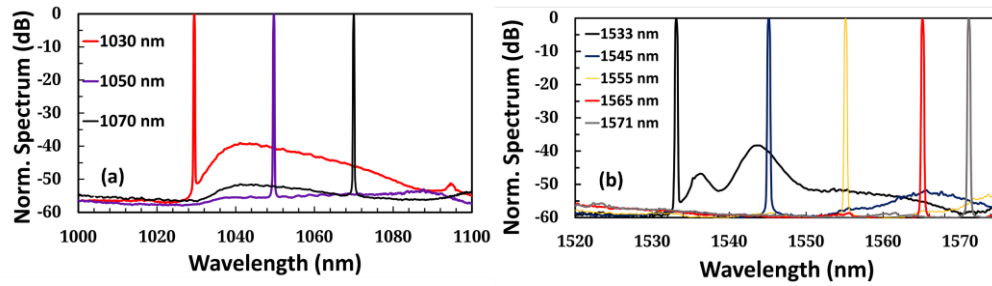


Fig. 2. Spectra showing the tuning range with 10 W output power around a) 1050 nm and b) 1550 nm [19]. The OSA resolution is 0.1 nm.

been measured by sweeping the oven temperature around the phase matching condition with a step of 0.2 °C.

3. Results and discussion

3.1. Tunability and power scaling

Considering the extreme wavelengths that can be reached by our pump systems (1030 + 1533 nm and 1070 + 1571 nm), we can expect to achieve a tunability in the visible from 616 nm to 636 nm. However, we are limited by the crystal: taking into account the values of Λ and the oven temperature span, a tuning range between 616.5 nm (sum of 1030 nm and 1536 nm at 32 °C) and 630.8 nm (sum of 1054 nm and 1571 nm at 245 °C) can be obtained. Four combinations were used to achieve four wavelengths in the visible between 616.5 nm and 630.8 nm, and their corresponding experimental parameters are summarized in Table 1. The phase matching temperature values obtained experimentally and shown in Table 1, are in agreement with the values calculated using phase mismatch and Sellmeier equations [4,11] with less than 1% difference. It is worth mentioning that the switch between the channels is ensured by moving manually the crystal along the X axis (Fig. 1).

Table 1. Tunability parameters

Visible wavelength nm	Infrared wavelengths nm		Phase matching conditions	
	Pump 1 nm	Pump 2 nm	Pitch μm	Oven temperature °C
616.5	1030	1536	11.12	32
622.12	1030	1571	11.22	117
626.5	1042	1571	11.22	185
630.8	1054	1571	11.22	245

The power scaling at these four wavelengths is presented in Fig. 3(a). A fixed power of 7 W at 1.5 μm (1536 nm or 1571 nm depending on the generated wavelength), is coupled within the crystal and the power at 1 μm (1030 nm or 1054 nm) is varied from 1 W to 10 W. An output power between 6.7 W and 7 W has been obtained at 616.5 nm (plotted in blue), 622.12 nm (plotted in red) and 626.5 nm (plotted in orange) for 17 W of total input power, reaching a maximum optical-optical efficiency (η) of 41% and a normalized nonlinear conversion efficiency of $2.5\% \text{W}^{-1} \text{cm}^{-1}$. This efficiency matches the current state of the art at this power level [5]. The theoretical nonlinear conversion efficiency for 40 mm crystal length is $3.5\% \text{W}^{-1} \text{cm}^{-1}$ [14]. With 1 W pump each at 1030 nm and 1536 nm, we obtained 140 mW of red emission which corresponds

to $3.5\% \text{ W}^{-1}\text{cm}^{-1}$ conversion efficiency. However, during power scaling the conversion efficiency is expected to be lower because of pump depletion and thermal effects. It is worth noting that the input power is measured between M2 and L3 without taking into consideration the losses on L3 and the input facet of the crystal which are measured to be 2% at both infrared wavelengths. Unfortunately, a decrease of output power is noticed at 630.8 nm where the maximum output power reached is 5.4 W corresponding to an efficiency of 32% ($2\% \text{ W}^{-1}\text{cm}^{-1}$). This drop in power can be related to an inhomogeneous heat distribution inside the crystal when the temperature of the oven becomes as high as 245 °C. The far field intensity distributions obtained for the maximum output powers are depicted in the insets of Fig. 3(a), and they all show a gaussian profile.

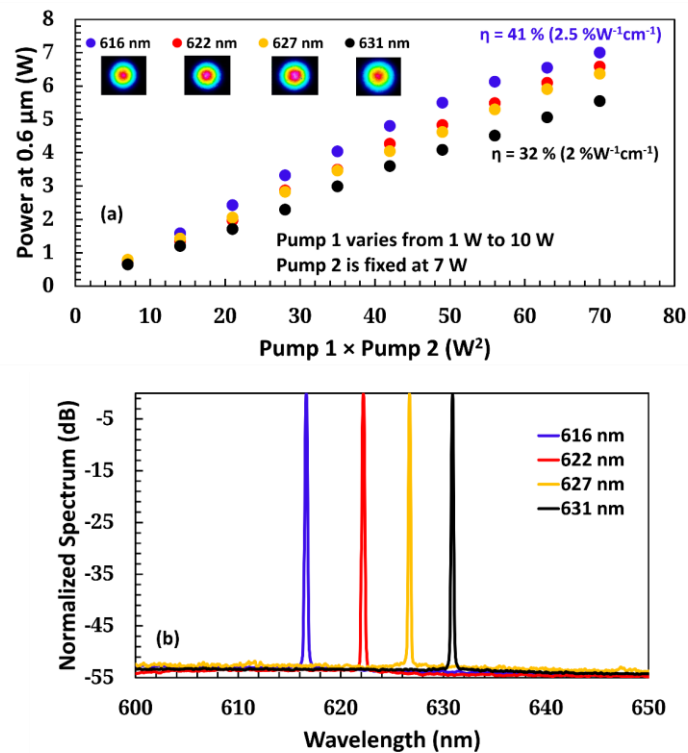


Fig. 3. (a) Power scaling at four different wavelengths with the beam profile obtained at maximum output power for each wavelength. The input power at 1.5 μm is fixed at 7 W and the input power at 1 μm is varied from 1 W to 10 W. (b) Emitted spectrum obtained at each wavelength of Fig. 3(a) at its maximum output power. The OSA resolution is 0.05 nm.

The optical spectrum of each wavelength of Fig. 3(a) at the maximum output powers is depicted in Fig. 3(b). The resolution of the OSA is 0.05 nm (with a span of 50 nm). An OSNR of 55 dB (limited by the dynamic range of the OSA) is measured for all wavelengths, which means that the ASE observed in the amplifier spectra (Fig. 2) is filtered out by the spectral acceptance of the crystal. A wide tunability of 14.3 nm is demonstrated with an output power ranging from 5 to 7 W for 17 W of total pump power. This represents the widest tuning range demonstrated in the orange/red spectral band at such high-power level in the single frequency regime.

After the demonstration of the tunability property of our laser, we studied the power scaling of our system and were able to exceed the 10 W level at a fixed wavelength. To the best of our knowledge, this is the highest power reported in ultra-low noise single frequency regime in the

red spectrum. To achieve this high-power level, the output power of the MOPAs were boosted to their maxima. Therefore, the seed laser wavelength in pump 1 and pump 2 was adjusted to 1042 nm and 1562 nm respectively, as they correspond to the gain central wavelengths of each MOPA. At these wavelengths, an output power of 12 W can be achieved at 1042 nm and the power at 1562 nm can reach 11 W. Under these conditions, a fixed power of 10.5 W at 1562 nm was coupled into the crystal and the power at 1042 nm was varied from 1 W to 12 W with a step of 1 W. The evolution of the output power (black) and the normalized nonlinear conversion efficiency (blue) at 624.5 nm are shown in Fig. 4. A maximum output power of 10.1 W is measured for 12 W at 1042 nm (22.5 W of total power). Moreover, the opt-opt efficiency increases from 9% to 45% at maximum input power, while the normalized nonlinear conversion efficiency decreases from $2.5\%W^{-1}cm^{-1}$ to $1.98\%W^{-1}cm^{-1}$ because of pump depletion and thermal effects. Additionally, the beam profile was measured at full power and a Gaussian intensity distribution is obtained. Moreover, the spectrum measured with 0.02 nm resolution shows an OSNR of 60 dB.

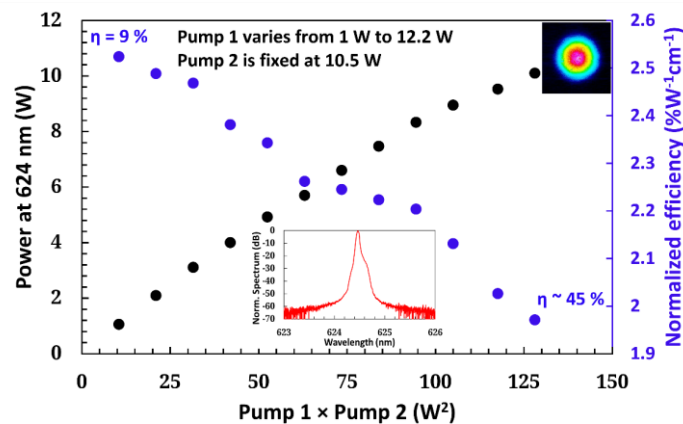


Fig. 4. Evolution of output power at 624.5 nm (black) and normalized conversion efficiency (blue) with the variation of pump 1 \times pump 2 for a fixed pump 2 power of 10.5 W. Inset: beam profile at full output power and spectrum at 624.5 nm with an OSA resolution of 0.02 nm.

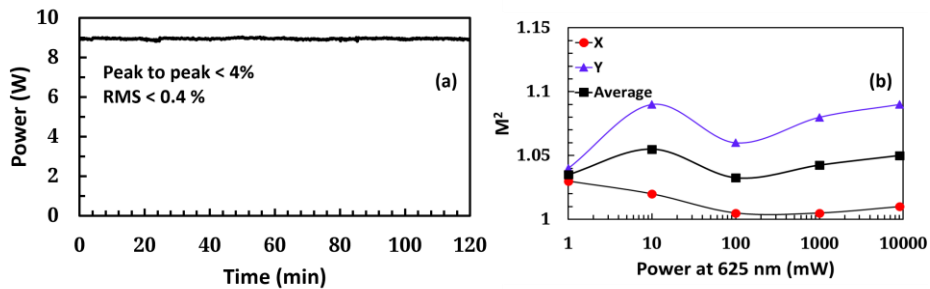


Fig. 5. (a) Time stability measurement at 9 W for 2 hours. (b) M^2 value at different power levels between 1 mW and 9 W.

It is worth noting that material degradation was observed on the silver mirror M2 at 22.5 W due to the relatively small size of the beams (equivalent to a power density exceeding $2\text{ kW}/\text{cm}^2$), thus the power of pump 1 was reduced slightly to correspond to a visible output power of 9 W. The stability of the laser at 9 W was monitored for over two hours of operation and shows a

stable behavior with peak-to-peak fluctuation less than 4% and RMS fluctuation lower than 0.4% (Fig. 5(a)). Moreover, the output beam quality was evaluated at 1 mW, 10 mW, 100 mW, 1 W, and 9 W using M^2 technique (Fig. 5(b)) and values between 1 and 1.1 were obtained over x (red) and y (blue) axis with an average of 1.05 at all power levels which highlights the good beam quality of our laser.

3.2. RIN investigation

Besides the tunability, one of the key features of the laser presented in this work is its ultra-low intensity noise. The RIN of single pass SHG-based lasers has been investigated in recent works [20,21]. However, to the best of our knowledge, the evolution of the RIN of the lasers realized by SFG has never been studied. In this section, a simple analytical model describing the behavior of the RIN in SFG process is presented. Thereafter, the analytical prediction is evaluated by measuring the RIN of the red emission, in different configurations.

During SFG, if we suppose that our laser is operating in quadratic regime, the following equations can be used to describe the relation between the power of the three interacting beams:

$$P_{\omega_3} = \eta P_{\omega_1} P_{\omega_2} \quad (1)$$

$$\delta P_{\omega_3} = \eta P_{\omega_2} \delta P_{\omega_1} + \eta P_{\omega_1} \delta P_{\omega_2} \quad (2)$$

Where P_{ω_1} , P_{ω_2} , and P_{ω_3} are the powers of pump 1, pump 2, and the generated signal, and η is the nonlinear conversion efficiency and δP the power fluctuations. Mathematically, the power fluctuations described in eq. (2) is the derivation of eq. (1).

Moreover, the RIN at each wavelength can be defined as following:

$$RIN_{\omega_i} = \frac{\langle \delta P_{\omega_i} \rangle^2}{P_{\omega_i}^2} \quad (3)$$

With $i = 1, 2$ or 3 .

Using the relations (2) and (3), the RIN_{ω_3} can be written as follow:

$$RIN_{\omega_3} = RIN_{\omega_1} + RIN_{\omega_2} + 2 \frac{\langle \delta P_{\omega_1} \delta P_{\omega_2} \rangle}{P_{\omega_1} P_{\omega_2}} \quad (4)$$

We can consider that SHG is a particular case of SFG where $\omega_1 = \omega_2$. Thus, in SHG the RIN of the generated signal is 4 times (equivalent to 6 dB) higher than the RIN of the fundamental laser [20]. However, in SFG the pump lasers differ in wavelengths therefore the noise of the used lasers is statistically independent which annihilates the last term of Eq. (4). Therefore, the noise of the generated signal in this case will be the sum of the noise of the two pump lasers. This also means that when the pump lasers have the same noise value ($RIN_{\omega_1} = RIN_{\omega_2}$), The RIN_{ω_3} will have an increase of 3 dB compared to RIN_{ω_1} and RIN_{ω_2} .

The analytical prediction obtained above is evaluated by experimentally investigating the RIN at different wavelengths, power levels and pump power ratio values. We define $\alpha = P_{\omega_1}/P_{\omega_2}$ as the ratio between the power of pump 1 (at 1 μm) and the power of pump 2 (at 1.5 μm). The RIN measurement is realized using a homemade low noise photodetector with a fast Fourier transform analyzer. The photocurrent from the photodetector was adjusted to be 6 mA at all wavelengths. Under these conditions, our current shot noise limit can reach a value of -163 dB/Hz. It is known that in fiber amplifiers, the pump and the environmental perturbations have a major impact at low frequencies (below 100 kHz), while the intensity noise at high frequencies (beyond 100 kHz) depends on the seed laser and the MOPA properties like the ASE and the stimulated Brillouin scattering [17,22,23] and the transition between the two regimes follows a smooth decay described by a first-order transfer function which depends on the power and

the gain medium properties (i.e., the active fiber) such as the ions lifetime, the absorption and emission cross sections [23]. Figure 6 shows the measured RIN of pump 1 at 10 W (blue curve), pump 2 at 7 W (black curve) and the SFG output signal at 7 W (red curve) at 616.5 nm ($\alpha=1.5$) and the analytical prediction of the RIN of the SFG (gray curve) by summing the RINs of infrared lasers. An excellent agreement between the analytical predicted curve and the measured one is obtained. Figure 6 shows that for frequencies between 100 kHz and 500 kHz, pump 2 has a RIN 10 dB lower than pump 1, and the RIN of the red laser follows the noisier laser (i.e., the RIN of pump 1). However, at 16 kHz we can notice that the RINs of the infrared lasers intersect and an increasing of 3 dB is observed on the RIN of red laser (inset Fig. 6). Moreover, for frequencies higher than 2 MHz, the RIN of pump 1 and pump 2 reach the same level (the difference of less than 1 dB is due to shot to shot measurement fluctuations) around -159 dB/Hz. This value is a little bit higher than the shot noise limit because of the presence of small amount of ASE at 1030 nm and 1536 nm (see Fig. 2). Beyond 2 MHz, an increase of 2 dB in the red laser RIN is observed instead of 3 dB expected theoretically. The slight 1 dB difference between the experimental and the analytical prediction curve can be attributed to measurement fluctuation or by the ASE filtering within the crystal (neglected in the analysis). At 5 MHz, the red radiation operating at 616.5 nm and at 7 W output power provides a RIN value as low as -157 dB/Hz.

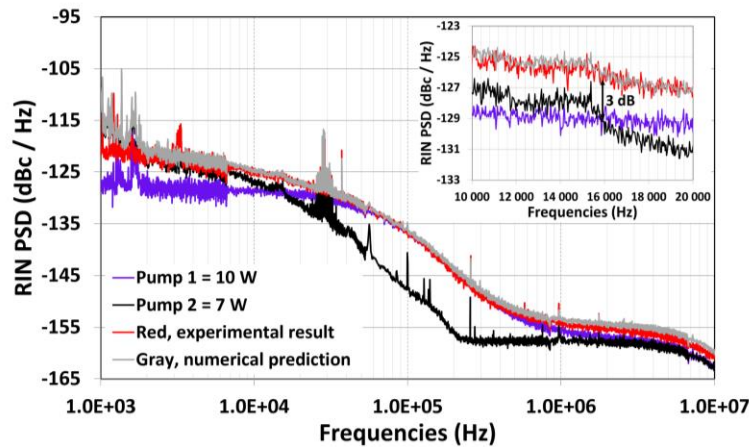


Fig. 6. RIN measurement of pump 1 (blue), pump 2 (black), and red laser (red) at 616.5 nm at 10 W, 7 W, and 7 W output power respectively. The RIN predicted for the red radiation is presented in gray. Inset: zoom-in around 16 kHz where the two pumps intersect.

Now we will investigate the intensity noise of SFG at low power of 200 mW at 630.8 nm in two different situations. In the first one, 4.3 W at 1571 nm and 0.614 W at 1054 nm were coupled within the crystal, which gives an α value of 0.142. The result presented in Fig. 7(a) shows that the curve of red emission (red) perfectly matches the curve of pump 1 (blue) over the entire frequency range (100 Hz-10 MHz) because pump 2 has a lower intensity noise compared to pump 1. While in the second configuration (Fig. 7(b)), where the power of pump 1 is increased up to 5.85 W and the power of pump 2 is reduced to 0.4 W (giving an α value of 14.6), the red curve overlays with the black curve (RIN of pump 2) at low frequencies (100 Hz-10 kHz) and then it starts to match the blue curve (RIN of pump 1) from 60 kHz. Indeed, the reduction of 1.5 μ m pump power induces an increase of the RIN at low frequencies, due to unoptimized operating conditions of the 940 nm pump diodes. Moreover, we can see in Fig. 7(b) that when the curves of both pumps intersect (which means that both input signals have the same intensity noise value) at 17 kHz, a difference of 3 dB is measured (Inset Fig. 7(b)) between the input and the output signals which corresponds to the sum of two pumps noise. Therefore, the results shown in Fig. 7,

demonstrate again that the RIN of the SFG output signal, overlays with the noisier pump and it increases when the noise of the pumps become closer until it gains a factor of 3 dB when they are exactly equal.

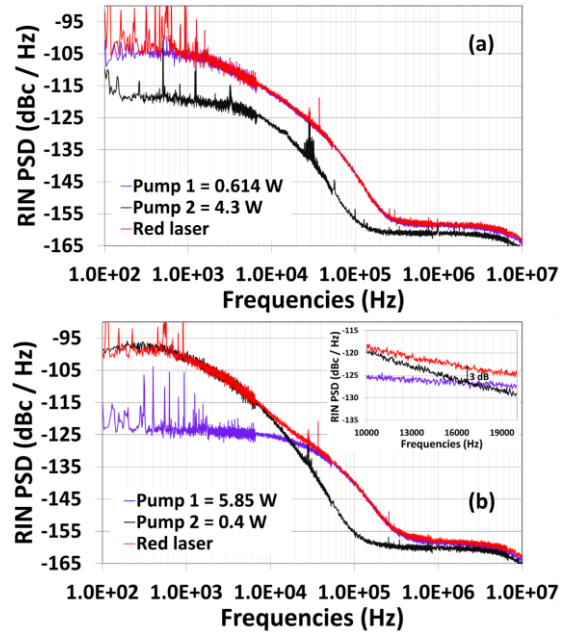


Fig. 7. RIN measurement of pump 1 (1054 nm, blue), pump 2 (1571 nm, black), and red emission (630.8 nm, red) at 200 mW output power when (a) $\alpha = 0.142$ and (b) $\alpha = 14.6$ (inset: zoom-in around 17 kHz where the two pumps intersect).

Figure 8 depicts the RIN obtained at 624.5 nm at 9 W power and shows an intensity noise level between -158 dB/Hz at 1 MHz and -160 dB/Hz at 5 MHz. The power of pump 1 and pump 2 is 10 W and 10.5 W respectively (see Fig. 4) which corresponds to an α value close to 1. To the best of our knowledge, this is the first demonstration of such ultra-low intensity noise property in the red band at this power level.

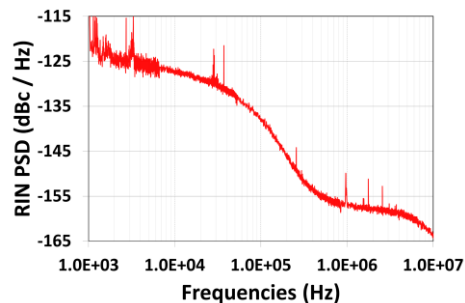


Fig. 8. RIN measurement of red emission (624.5 nm) at 9 W output power with $\alpha \sim 1$.

4. Conclusion

We have demonstrated a 14 nm tunable single frequency laser with more than 5 W of output power. The laser spans from 616.5 nm in the orange spectral band to 630.8 nm in the red band using two homemade tunable low-noise MOPAs around 1050 nm and 1550 nm. Moreover, a maximum output power of 10.1 W and an opt-opt efficiency of 45% have been demonstrated at 624.5 nm. The ultra-low RIN of the visible laser, investigated at several wavelengths and at different power levels, shows that it is the sum of the intensity noise of pump lasers. In other words, it overlays the infrared laser which has the higher noise and increases by 3 dB when the infrared lasers have the same noise level.

Funding. Agence Nationale de la Recherche (LAPHIA (ANR-10-IDEX-03-02)); Région Nouvelle Aquitaine (project n°2019-1R50301).

Acknowledgments. The authors acknowledge J. H. Codarbox, P. Teulat and A. Tizon for their technical support. The authors acknowledge financial supports from the French National Research Agency (ANR) in the frame of “the investments for the future” Program IdEx Bordeaux – LAPHIA (ANR-10-IDEX-03-02).

Disclosures. The authors declare no conflicts of interest

Data availability. Data underlying the results presented in this paper are not publicly available at this time but may be obtained from the authors upon reasonable request.

References

1. J.-B. Trebbia, P. Tamarat, and B. Lounis, “Indistinguishable near-infrared single photons from an individual organic molecule,” *Phys. Rev. A* **82**(6), 063803 (2010).
2. A. M. Hankin, Y.-Y. Jau, L. P. Parazzoli, C. W. Chou, D. J. Armstrong, A. J. Landahl, and G. W. Biedermann, “Two-atom Rydberg blockade using direct 6S to nP excitation,” *Phys. Rev. A* **89**(3), 033416 (2014).
3. A. C. Wilson, C. Ospelkaus, A. P. VanDevender, J. A. Mlynek, K. R. Brown, D. Leibfried, and D. J. Wineland, “A 750-mW, continuous-wave, solid-state laser source at 313 nm for cooling and manipulating trapped 9Be^+ ions,” *Appl. Phys. B* **105**(4), 741–748 (2011).
4. E. M. Bridge, N. C. Keegan, A. D. Bounds, D. Boddy, D. P. Sadler, and M. P. A. Jones, “Tunable cw UV laser with <35 kHz absolute frequency instability for precision spectroscopy of Sr Rydberg states,” *Opt. Express* **24**(3), 2281–2292 (2016).
5. H.-Y. Lo, J. Alonso, D. Kienzler, B. C. Keitch, L. E. de Clercq, V. Negnevitsky, and J. P. Home, “All-solid-state continuous-wave laser systems for ionization, cooling and quantum state manipulation of beryllium ions,” *Appl. Phys. B* **114**(1-2), 17–25 (2014).
6. P. Thoumany, T. Hänsch, G. Stania, L. Urbonas, and Th. Becker, “Optical spectroscopy of rubidium Rydberg atoms with a 297 nm frequency-doubled dye laser,” *Opt. Lett.* **34**(11), 1621–1623 (2009).
7. R. Beigang, K. Lücke, D. Schmidt, A. Timmermann, and P. J. West, “One-photon laser spectroscopy of Rydberg series from metastable levels in calcium and strontium,” *Phys. Scr.* **26**(3), 183–188 (1982).
8. J.-Y. Wang, J.-D. Bai, J. He, and J. Wang, “Development and characterization of a 2.2 W narrow-linewidth 318.6 nm ultraviolet laser,” *J. Opt. Soc. Am. B* **33**(10), 2020–2025 (2016).
9. R. J. Rengelink, R. P. M. J. W. Notermans, and W. Vassen, “A simple 2 W continuous-wave laser system for trapping ultracold metastable helium atoms at the 319.8 nm magic wavelength,” *Appl. Phys. B* **122**(5), 122 (2016).
10. Zu Hubner photonics, “Widely tunable continuous-wave lasers,” <https://hubner-photonics.com/products/lasers/tunable-lasers/c-wave/>.
11. Covesion resources, “Material properties of Lithium Niobate,” <https://www.covesion.com/en/resource/material-properties-of-lithium-niobate/>, (Covesion, 2020).
12. T. H. Runcorn, R. T. Murray, and J. R. Taylor, “High average power second-harmonic generation of a CW erbium fiber MOPA,” *IEEE Photonics Technol. Lett.* **29**(18), 1576–1579 (2017).
13. J. Dong, X. Zeng, S. Cui, J. Zhou, and Y. Feng, “More than 20 W fiber-based continuous-wave single frequency laser at 780 nm,” *Opt. Express* **27**(24), 35362 (2019).
14. J. Y. Wang, J. D. Bai, J. He, and J. M. Wang, “Realization and characterization of single-frequency tunable 637.2 nm high-power laser,” *Opt. Commun.* **370**, 150–155 (2016).
15. D. Darwich, Y.-V. Bardin, M. Goepfner, C. Dixneuf, G. Guiraud, N. Traynor, G. Santarelli, and A. Hilico, “Ultralow-intensity noise, 10 W all-fiber single-frequency tunable laser system around 1550 nm,” *Appl. Opt.* **60**(27), 8550–8555 (2021).
16. B. Gouhier, C. Dixneuf, A. Hilico, G. Guiraud, N. Traynor, and G. Santarelli, “Low Intensity Noise High-Power Tunable Fiber-Based Laser Around 1007 nm,” *J. Lightwave Technol.* **37**(14), 3539–3543 (2019).
17. D. Darwich, Y.-V. Bardin, M. Goepfner, C. Dixneuf, G. Guiraud, N. Traynor, G. Santarelli, and A. Hilico, “Influence of pump properties on the tunability of 1.5 μm low-noise single frequency fiber amplifier,” *IEEE Photon. Technol. Lett.* **34**(1), 27–30 (2022).

18. G. Boyd and D. Kleinman, "Parametric interaction of focused gaussian light beams," *J. Appl. Phys.* **39**(8), 3597–3639 (1968).
19. O. Gayer, Z. Sacks, E. Galun, and A. Arie, "Temperature and wavelength dependent refractive index equations for MgO-doped congruent and stoichiometric LiNbO₃," *Appl. Phys. B* **91**(2), 343–348 (2008).
20. R. Collin, T. Chartier, and P. Besnard, "Numerical investigation of relative intensity noise in frequency-doubled multimode fiber lasers," *Opt. Commun.* **485**, 126724 (2021).
21. C. Dixneuf, G. Guiraud, H. Ye, Y.-V. Bardin, M. Goepfner, G. Santarelli, and N. Traynor, "Robust 17 W single-pass second-harmonic-generation at 532 nm and relative-intensity-noise investigation," *Opt. Lett.* **46**(2), 408–411 (2021).
22. H. Tünnermann, J. Neumann, D. Kracht, and P. Weßels, "Gain dynamics and refractive index changes in fiber amplifiers: a frequency domain approach," *Opt. Express* **20**(12), 13539 (2012).
23. J. Zhao, G. Guiraud, F. Floissat, B. Gouhier, S. Rota-Rodrigo, N. Traynor, and G. Santarelli, "Gain dynamics of clad-pumped Yb-fiber amplifier and intensity noise control," *Opt. Express* **25**(1), 357 (2017).